Polymer Journal, Vol. 39, No. 1, pp. 73–80 (2007)
©2006 The Society of Polymer Science, Japan

Molecular Dynamics Study of the Adhesion between End-Grafted Polymer Films II —Effect of Grafting Density—

Hiroshi MORITA,[1,†] Haruki MIURA,[2] Masamichi YAMADA,[2]
Tetsuo YAMAGUCHI,[1] and Masao DOI[1]

[1]*Japan Science and Technology Agency & Department of Applied Physics, The University of Tokyo, 7-3-1 Hongo, Bunkyo-ku, Tokyo 113-8656, Japan*
[2]*Department of Computational Science and Engineering, Nagoya University, Furo-cho, Chikusa-ku, Nagoya, 464-8603, Japan*

(Received August 17, 2006; Accepted October 31, 2006; Published December 7, 2006)

ABSTRACT: Adhesion between two polymer films consisting of end grafted polymer is studied by coarse-grained molecular dynamics. The grafting density of the polymer film is varied from the dilute mushroom region to dense polymer brush region, and the debonding behavior is studied by varying the temperature. It is shown that below the glass transition temperature, the debonding behavior is mainly determined by grafting density. At low grafting density, fibrils are formed and the stress-strain curve has a plateau region. At high grafting density, the fracture becomes brittle like, and the stress drops sharply after the strain exceeds certain critical values. Above the glass transition temperature, cavities are formed, and the stress becomes a gradually decreasing function of strain. [doi:10.1295/polymj.PJ2006095]

KEY WORDS Coarse-Grained Molecular Dynamics Simulation / OCTA / Grafted Polymer Film / Grafting Density /

Adhesion is an important property in various applications of polymers. Despite its importance, fundamental study of adhesion has just begun, as it is reviewed by Creton *et al.*[1] In such studies, end grafted polymer film has been used since its structure can be controlled. Experimental study of the adhesion of end-grafted polymer has been done by Leger and her collaborators.[2,3]

In the previous paper,[4] we reported the result of computer simulation for the debonding process of end-grafted polymer. We have shown that the glass transition temperature is quite important in determining the stress-strain curve in the debonding process. The simulation, however, was done only for a particular grafting density. In this paper, we shall report the result for various grafting density and discuss how the grafting density changes the debonding behavior.

It has been shown that the structure of the end-grafted polymer changes significantly as the grafting density is changed.[6] Milner *et al.* calculated the depth density profile of grafted polymers using mean field theory.[5] At low grafting density, the polymers are separated from each other, and the structure is called the "mushroom". With the increase of the grafting density, the polymer chain overlaps each other, and the structure gradually changes to the "brush". Murat and Grest[7–9] studied the three dimensional chain structures of grafted polymers using coarse-grained molecular dynamics simulations, and confirmed the "mushroom" and the "brush" structures. Our interest here was how this structural change affects the adhesion property.

Recently, there are an increasing number of molecular dynamics studies for polymer surfaces. Glass transition temperature of polymer thin film and polymer surface has been studied by Baljon *et al.*[10] and Morita *et al.*,[11] respectively. The rheological properties of polymer thin film has been studied by de Pablo *et al.*[12] Morita *et al.*[13] studied the adhesion and friction between polymer and AFM tip. These works are for polymer melts. The grafted polymer film has been studied by Sides *et al.*,[14–16] but they have done simulation only for one grafting density.

We conducted the molecular dynamics simulation for the debonding process by varying the temperature and grafting density over a wide range. Our aim was to construct an overall picture for the type of the stress-strain curve and the structural change during the debonding process.

MODEL

The model and the molecular dynamics (MD) simulation method are same as in the previous study.[4] We used the bead spring chain for the model of the grafted polymer.[7,8,17,18] Simulations are performed using the molecular dynamics program COGNAC in the OCTA system.[19,20]

†To whom correspondence should be addressed (E-mail: hmorita@rheo.t.u-tokyo.ac.jp).

The film of the straight polymer involves 81 chains, each consisting of 40 beads of mass m. As the entanglement molecular weight of the bead-spring chain is about 30–40 beads,[18] we consider that the entanglement between upper and lower films does not occur in this system. The grafted points are placed regularly on the square lattice with the neighboring distance ℓ_S. In this study, ℓ_S is changed from 1.12σ to 5.0σ, where σ is the van der Waals diameter of the beads (see eq 3).

The interaction potential used in the simulation is as follows. For the bonded beads, FENE-LJ potential is assumed.

$$U^B(r) = U^{FENE}(r) + U^{LJ}(r) \tag{1}$$

$$U^{FENE}(r) = \begin{cases} -\frac{1}{2}kR_0^2 \ln\left(1 - \left(\frac{r}{R_0}\right)^2\right), & (r \le R_0) \\ \infty, & (r > R_0) \end{cases} \tag{2}$$

$$U^{LJ}(r) = \begin{cases} 4\varepsilon\left[\left\{\left(\frac{\sigma}{r}\right)^{12} - \left(\frac{\sigma}{r}\right)^{6}\right\} - \left\{\left(\frac{\sigma}{r_{cut}}\right)^{12} - \left(\frac{\sigma}{r_{cut}}\right)^{6}\right\}\right], & (r \le r_{cut}) \\ 0, & (r > r_{cut}) \end{cases} \tag{3}$$

where r is the bead-bead distance, r_{cut} is the cut off distance, k is the spring constant, and R_0 is the maximum extension of the spring, ε is the strength of the interaction. For the non-bonded beads, only the LJ part of the potential is assumed. As we set $r_{cut} = 5.0\sigma$, there is an attractive interaction between non-bonding beads. The interaction between beads and the wall is expressed by the integrated van der Waals potential:

$$U^{Wall}(z) = 4\varepsilon_w\left[\frac{1}{5}\left(\frac{\sigma_w}{z}\right)^{10} - \frac{1}{2}\left(\frac{\sigma_w}{z}\right)^{4}\right] \tag{4}$$

where z is the distance between the wall and the bead, and ε_w is the strength of the interaction.

We took m, σ and ε as the unit of mass, length and energy respectively. The unit of time τ, and the unit of the temperature T_0 are defined by

$$\tau = \sigma(m/\varepsilon)^{1/2}, \quad T_0 = \varepsilon/k_B$$

The temperature T was changed in the range $0.1[T_0] < T < 1.0[T_0]$ and Γ is taken to be $0.5[\tau^{-1}]$. The parameters characterizing the wall potential, ε_w and σ_w are taken to be $\varepsilon_w = \varepsilon$ and $\sigma_w = \sigma$.

RESULTS AND DISCUSSIONS

Structure of the Grafted Polymer Film

To prepare the initial structures of the grafted polymer film, we started from the completely stretched configuration of the grafted chains at very high temperature ($T = 2.0[T_0]$), and decreased the temperature gradually. At each temperature, we performed the simulation for at least 1,500,000 time steps to relax the system, and then continued the simulation for another 1,000,000 time steps to get the statistical data. We confirmed that in the last stage of the relaxation the thickness of the film and the total energy show no appreciable change in time.

Figure 1 shows the snapshot of the grafted polymer films for various grafting density $\rho_a = 0.001$, 0.01, 0.04, 0.1, 0.2, 0.4, $0.8[\sigma^{-2}]$ at $T = 1.0[T_0]$. In the lower grafting density, the configuration of the film takes the mushroom structure. There are two kinds of mushroom structures. At lowest grafting density, $\rho_a = 0.001[\sigma^{-2}]$, each chain constitutes one mushroom. At the grafting density of $\rho_a = 0.01$, $0.04[\sigma^{-2}]$, the

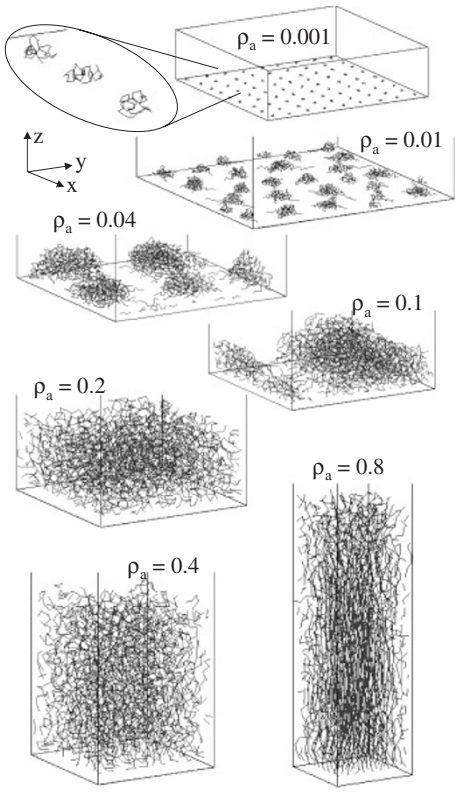

Figure 1. The snapshots of the grafted polymer at various grafting density.

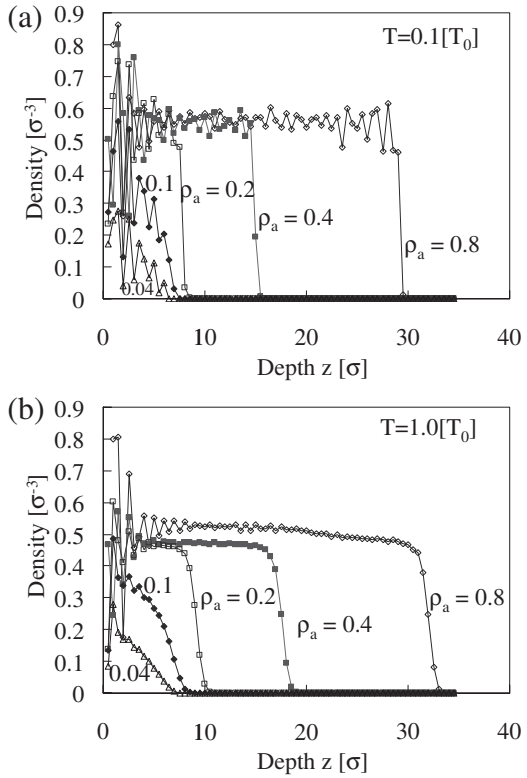

Figure 2. The segment density of the grafted polymers is plotted against the distance from the wall.

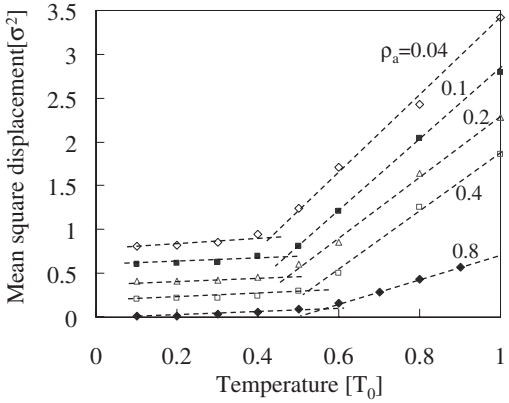

Figure 3. The mean square displacement of segments in a time interval $\Delta t = 25\tau$ is plotted against temperature (T). The grafting densities are $\rho_a = 0.04$, 0.1, 0.2, 0.4, and $0.8[\sigma^{-2}]$. The curves for the data of $\rho_a = 0.1$, 0.2, 0.4, and $0.8[\sigma^{-2}]$ are shifted vertically by 0.2, 0.4, 0.6, $0.8[\sigma^2]$ respectively to avoid the overlap.

chains aggregate to form large mushroom. This is due to the attractive interaction between beads. As the grafting density increase, the grafted chains take the film form and then change to stretched brush. At the highest grafting density, $\rho_a = 0.8[\sigma^{-2}]$, the chains are so strongly stretched out, that the structure looks like a extended chain crystal.

Figure 2 shows the density profiles at $T = 0.1[T_0]$ (a), and $1.0[T_0]$ (b). At the high grafting density, the profile has a constant density region and gradually decreasing region at surface. The film thickness at the density of $\rho_a = 0.8[\sigma^{-2}]$ is about $32[\sigma]$ and it is about 80% of the fully stretched length of the grafted polymer. At the low grafting density it is almost parabolic. The end-to-end distance of the free polymer with 40 beads is about $6.2[\sigma]$ in the bulk. The film thickness is about same as this distance at the density of $\rho_a = 0.04[\sigma^{-2}]$. In previous study, we choose the density $\rho_a = 0.14[\sigma^{-2}]$ and the chain constitute almost flat film.

Glass Transition Temperature of Grafted Polymer Film

We now discuss the glass transition temperature (T_g) of the grafted polymer film. In the previous study,[4] we estimated T_g by two methods: one is to study the film thickness as a function of temperature, and the other is to study the mean square displacement of each bead for a given time interval Δt as a function of temperature. We have shown that these two methods give almost the same value for T_g. We have also shown that the latter method can be used to estimate T_g of the bulk and T_g of the surface.[11] Since the film thickness of the mushroom structure cannot be defined, we used the latter method to estimate T_g: we calculated the mean square displacement (MSD) of beads in the short time interval, Δt:

$$\langle(\mathbf{r}(\Delta t) - \mathbf{r}(0))^2\rangle = \frac{1}{N}\sum_{n \neq \text{grafted beads}} \langle(\mathbf{r}_n(\Delta t) - \mathbf{r}_n(0))^2\rangle, \quad (5)$$

where N is the total number of beads not grafted on the wall.

Figure 3 shows MSD $\langle(\mathbf{r}(\Delta t) - \mathbf{r}(0))^2\rangle$ plotted against the temperature for various grafting density. The curves are shifted vertically in order not to overlap each other. The time Δt was taken to be 25τ, which is the same as that in the previous study.[4] This time interval is much longer than the mean collision time of beads, and is much smaller than the entanglement time τ_e. From this figure, we can determine the glass transition temperature as a breakpoint of each curve.

Figure 4 shows the glass transition temperature plotted against the grafting density. It is seen that as the grafting density increases, the glass transition temperature increases. This can be explained by the free volume theory.[21] With increasing the grafting density, the density of the film including the plateau region increases (see Figure 2b). This indicates that the free volume inside the film decreases and the glass transition temperature increases.

The grafting density also affects the mobility of

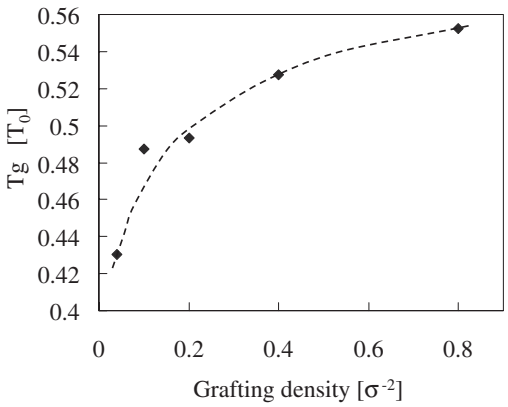

Figure 4. The glass transition temperature of the grafted films is plotted against the grafting density.

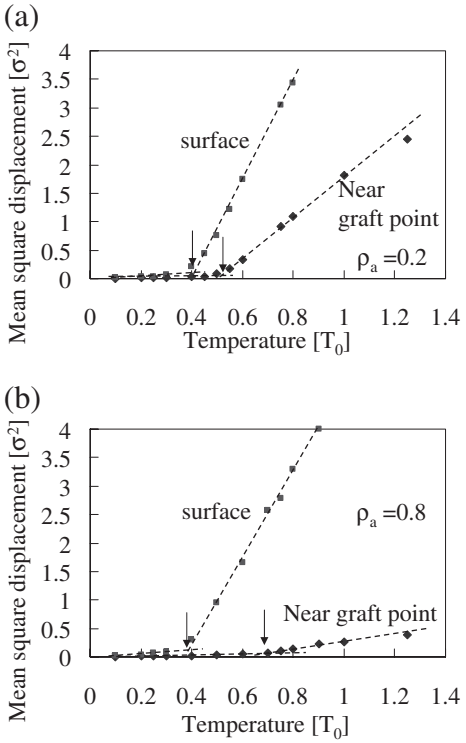

Figure 5. The mean square displacement of segments of limited regions of the surface and near graft in a time interval $\Delta t = 25\tau$ is plotted against temperature (T). Figures (a) and (b) show the data of $\rho_a = 0.2$ and $0.8[\sigma^{-2}]$, respectively.

beads inside the film. Using the technique described in ref 11, we evaluated the glass transition temperature of the surface. Figure 5 shows the mean square displacements of beads near the surface and that near the grafting point plotted against the temperature for the film of $\rho_a = 0.2$ and $0.8[\sigma^{-2}]$. The region near the surface and that near the grafting point are defined as the region of thickness about 2σ from the top of the film and that from the grafting point, respectively. From Figure 5, the glass transition temperatures at the surface (T_g^S) and near grafting point (T_g^G) are obtained by the break point of each curve. The T_g's shown in Figure 4 are between T_g^S and T_g^G. As the T_g^S is lower than the T_g^G, it is expected that beads at the surface region can relax faster than those near the grafting point.

Loading and Unloading Processes

Next we conducted the simulation for the loading and the unloading processes of the adhesion between two polymer films. We prepared two relaxed films by the same method described in the previous section and placed them face-to-face. The surfaces of the film were initially separated by the distance 1σ. The distance L_z between the two walls was then decreased at constant rate; this was done by changing ΔL_z by $2 \times 10^{-3}\sigma$ and displacing all beads affinely at every 20 time steps. Thus dL_z/dt is $-0.01\sigma/\tau$ in the loading process, and $0.05\sigma/\tau$ in the unloading process. The stress P acting on the wall was calculated by the total force acting on the wall:

$$P[m/\sigma\tau^2] = \frac{1}{S}\left(\sum_{grafted\ beads} F_{n,z} + \sum_{\neq grafted\ beads} F_{n,wall\text{-}beads}\right), \quad (6)$$

where S is the area of the wall, $F_{n,z}$ the z component of the force acting on the n-th grafted bead, and $F_{n,wall\text{-}beads}$ is the z component of the wall force acting on non-grafted beads n. The sign of the stress is taken to be such that it is positive when the wall is repelling each other. The loading process was stopped when the stress reaches the value $10.0[m/\sigma\tau^2]$, and then the unloading process was started immediately. Simulations were done at several temperatures $T = 0.1$–$1.0[T_0]$, and at several grafting density $\rho_a = 0.04$, 0.1, 0.2, 0.4, $0.8[\sigma^{-2}]$.

Figures 6, 7, and 8 show the typical stress-distance curves and snapshots in the loading and the unloading processes. The grafting density ρ_a and the temperature T are as follows. Figure 6: $\rho_a = 0.2[\sigma^{-2}]$ at $T = 0.1[T_0]$, Figure 7: $\rho_a = 0.2[\sigma^{-2}]$ at $T = 1.0[T_0]$, Figure 8: $\rho_a = 0.8[\sigma^{-2}]$ at $T = 0.1[T_0]$.

The failure mode of $\rho_a = 0.2[\sigma^{-2}]$ is similar to that reported in the previous study. At low temperature (Figure 6), fibrils are formed, and the stress remains constant over a long strain in the unloading process. At high temperature (Figure 7), cavities are formed, and the stress quickly decreases to zero. This behavior is qualitatively the same as that for $\rho_a = 0.14[\sigma^{-2}]$ reported in the previous study.

On the other hand, Figure 8 shows that there is a new kind of failure pattern at high grafting density. In the loading process, an attractive force appears sud-

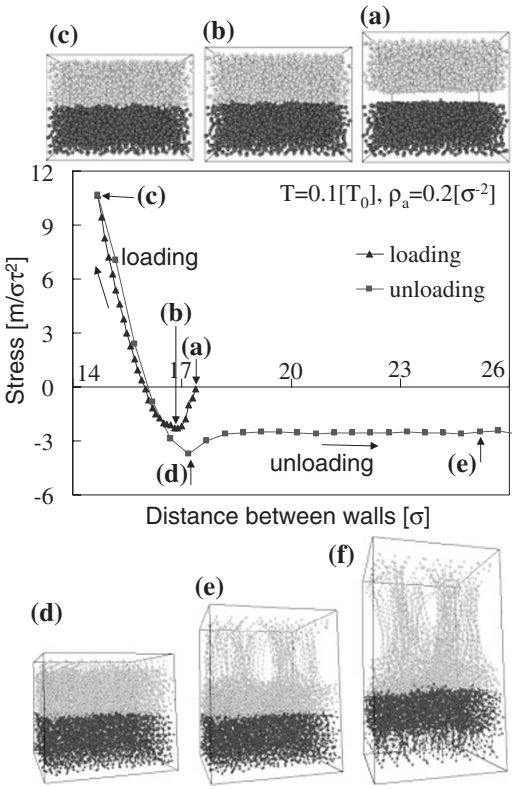

Figure 6. Stress-distance curves in the loading and the unloading processes. The snapshots of the molecular configuration are also shown. The temperature is $T = 0.1[T_0]$ and the grafting density is $0.2[\sigma^{-2}]$.

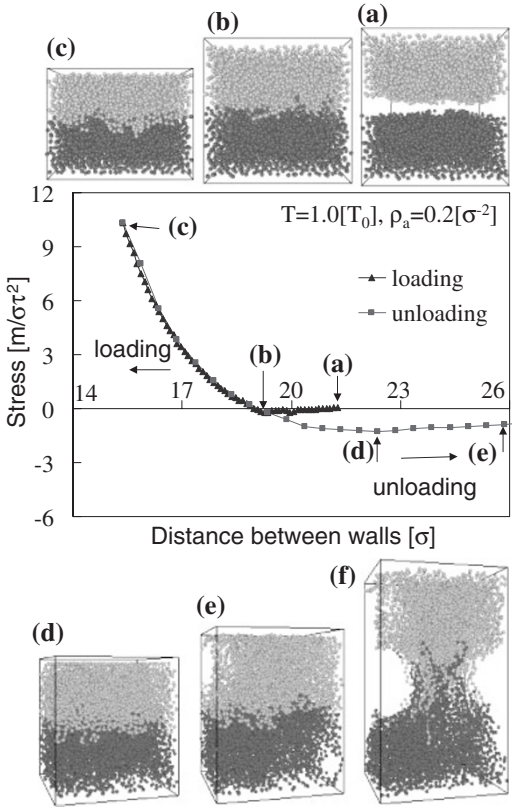

Figure 7. The same as in Figure 6. The temperature is $T = 1.0[T_0]$ and the grafting density is $0.2[\sigma^{-2}]$.

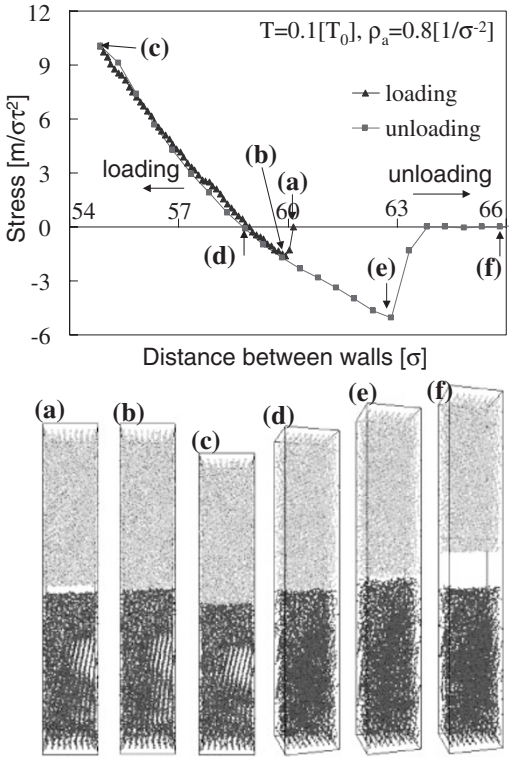

Figure 8. The same as in Figure 6. The temperature is $T = 0.1[T_0]$ and the grafting density is $0.8[\sigma^{-2}]$.

denly and it turns to be repulsive as the film is compressed. In the unloading process, the repulsive force decreases, turns to be attractive, and then suddenly jumps to zero at certain strain. The failure occurs suddenly. In the loading-unloading process, the structure of the film changes little in appearance. In the following, we shall call this mode brittle failure.

Figure 9 shows typical snapshots of the failing films for various temperature and grafting density. From this figure, we can distinguish three failure patterns, summarized in in Figure 10. The fibril failure is observed for low and intermediate grafting density at low temperature. The brittle failure is seen for high grafting density film and at low temperature. The cavity failure is observed at high temperature.

In the previous study, the failure patterns and the adhesion stress can be distinguished by the glass transition temperature. Though the phase boundary cannot be clearly shown in Figure 9, we also find that T_g is the important parameter to separate between fibril or brittle failures and cavity failure.

Bulk Modulus and Averaged Density of Grafted Polymer Film

The hardness (or softness) of the film is strongly influenced by the grafting density and it will affect the adhesion stress and the adhesion energy. Figure 11 shows the stress-distance curves in the loading process for two grafting density $\rho_a = 0.2[\sigma^{-2}]$ and $0.8[\sigma^{-2}]$.

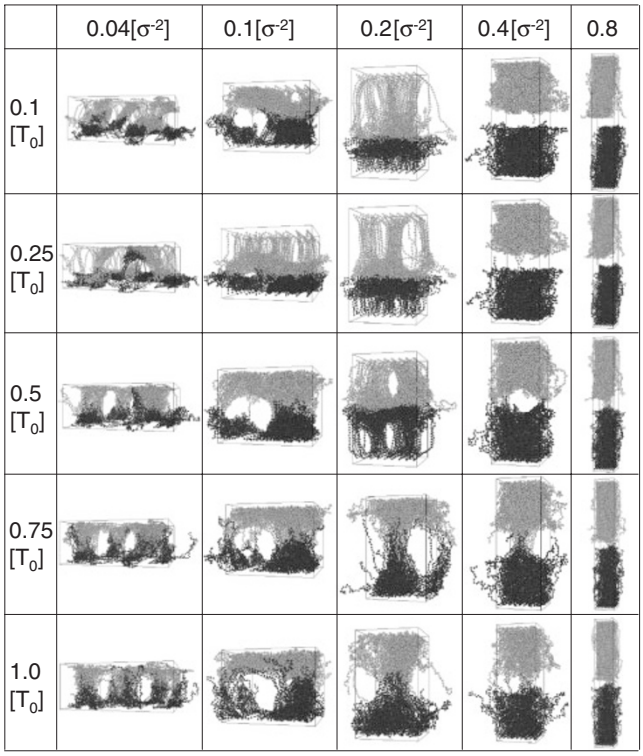

Figure 9. Chain configurations when the films are separated from each other in the unloading process with changing the temperature and the grafting density.

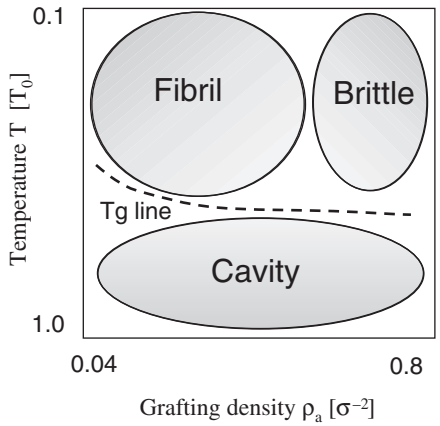

Figure 10. Schematic diagram of failure patterns in the parameter plane of temperature and grafting density. The regions of fibril, cavity and brittle failures are shown.

To quantify the hardness of the films, we obtained the apparent bulk modulus K defined as follows;

$$K = \frac{\Delta P}{\Delta V / V_{\text{initial}}},$$

where ΔP is the difference of the stress at selected two points, ΔV is the difference of the volume, and V_{initial} is the volume at $P = 0$. In this study, we chose the two points at $P = 0$ and $P = 10$ and calculated K.

Figure 12(a) shows the bulk modulus K plotted against the temperature. As the temperature increases,

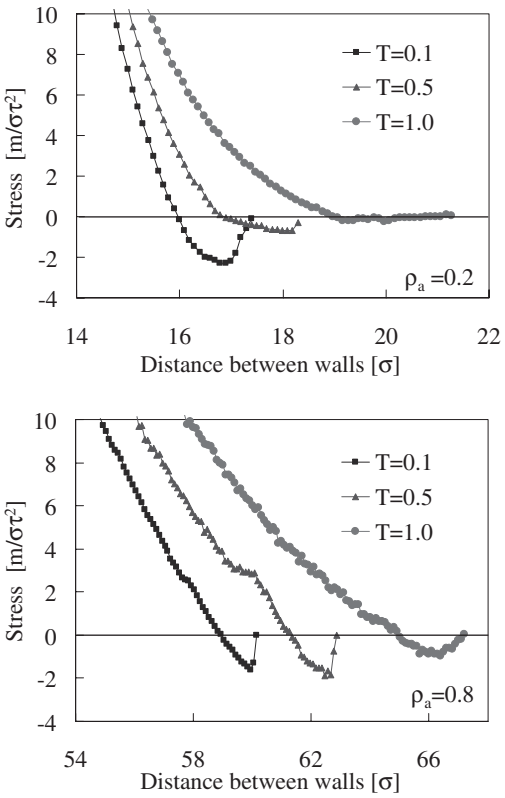

Figure 11. Stress-distance curves in the loading processes of adhesion between the grafted polymer films. The grafting density is $0.2[\sigma^{-2}]$ (top) and $0.8[\sigma^{-2}]$ (bottom).

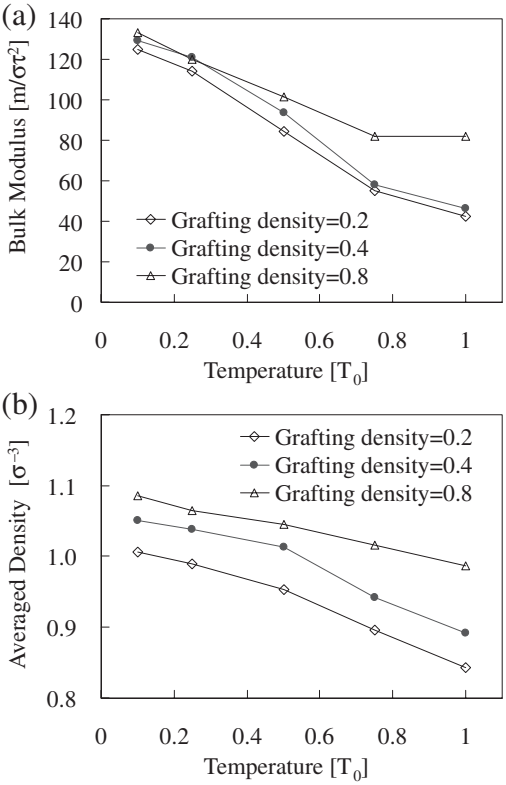

Figure 12. Bulk modulus and the average density are plotted against the reduced temperature for the grafting density of 0.2, 0.4 and $0.8[\sigma^{-2}]$.

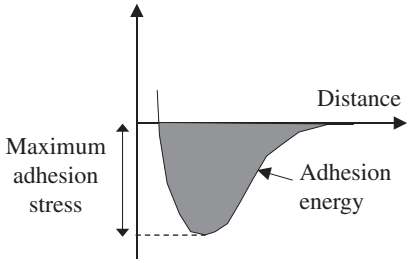

Figure 13. Definition of maximum adhesion stress and adhesion energy found in the unloading curve.

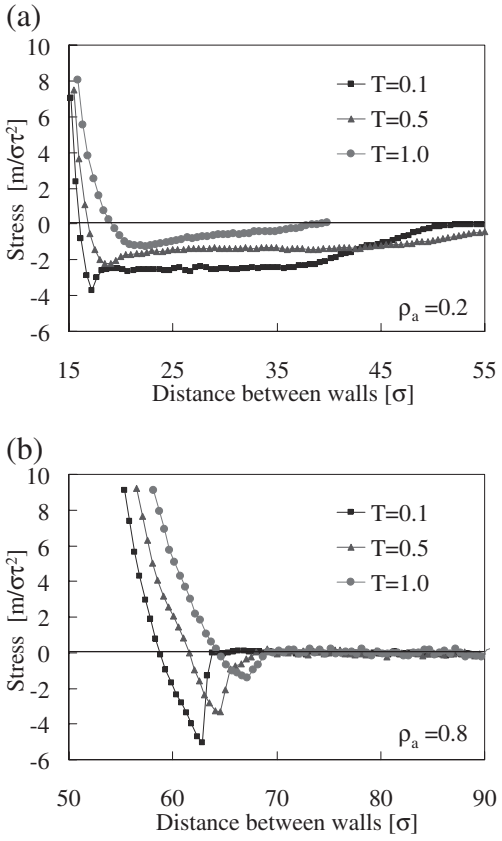

Figure 14. Stress-distance curves in the unloading processes of adhesion between the grafted polymer films, in which the grafting density are 0.2 and 0.8[σ^{-2}].

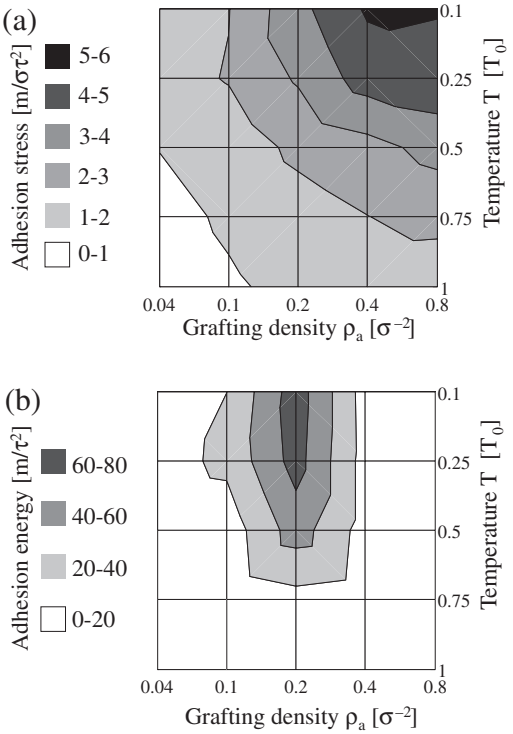

Figure 15. The maximum adhesion stress and the adhesion energy are shown as a function of the temperature and the grafting density. The definition of maximum adhesion stress and the adhesion energy is also indicated in Figure 13.

the bulk modulus decreases. The bulk modulus increases with the increase of the grafting density. Figure 12(b) shows the averaged density estimated by the volume at the time when stress turns from negative to positive. The density increases with the increase of the grafting density. Thus the film of high grafting density has little free space for each bead to move. In our simulation, the difference of the bulk modulus is not so large. We consider that this is due to the variation of the glass transition temperature across the film. As already shown in Figure 5, T_g^S is smaller than T_g^G, and T_g's shown in Figure 4 are between T_g^S and T_g^G. As the glass transition temperature varies across the film, the elastic modulus also varies across the film. Since the elastic modulus shown in Figure 12 primarily reflects the modulus near the surface, we think there is no drastic change in the bulk modulus.

Maximum Adhesion Stress and Adhesion Energy

We now discuss the maximum adhesion stress and the adhesion energy. The definitions of the maximum adhesion stress and the adhesion energy are given in Figure 13; the maximum adhesion stress is the maximum value of the attractive stress in the unloading process, and the adhesion energy is the work done by the attractive force in the unloading process. Notice that the distance at which the separation takes place is an important factor for the adhesion energy.

Figure 14 shows the stress-distance curve in the unloading process for the grafting density ρ_a 0.2[σ^{-2}] and 0.8[σ^{-2}]. In the low grafting density (Figure 14(a)), the distance in the attractive region is large and the film is strongly deformed before it fails. On the other hand, in the high grafting density (Figure 14(b)), the separation distance is quite small but the maximum adhesion stress is larger than that of the low grafting density.

Figure 15 shows a two dimensional plots of (a) the maximum adhesion stress and (b) the adhesion energy as a function of the temperature and the grafting den-

sity. Figure 15(a) shows that the largest adhesion stress is found in the region of brittle failure for high grafting density. This is not surprising since the adhesion stress is basically determined by the attractive LJ force between the beads of upper and lower films, and the stress increases with the increase of the segment density. On the other hand, the largest adhesion energy is found in the region of fibril failure as it is seen in Figure 15(b). In the case of the fibril failure, upper film can be detached from the lower film after a pulling for a long distance, which is effective for the larger adhesion energy.

CONCLUSION

In this paper, we have shown the results the of the molecular dynamics study of the adhesion between grafted polymer films with changing the grafting densities. We have shown that there are three kinds of failure patterns; fibril, cavity and brittle failures. The maximum adhesion stress and the adhesion energy are obtained from our MD simulations and these behaviors are strongly dependent on the temperature and the grafting density.

Our results indicate that the temperature and the grafting density are the important parameter to control the failure pattern, the adhesion stress, and the adhesion energy. The adhesion stress takes larger values in the case of higher grafting density below T_g of the film. On the other hand, the adhesion energy takes larger if the film takes lower grafting density below T_g of the film. As the grafting density increase, the film takes a high glass transition temperature and a high bulk modulus. These results are much concerned with the mobility of the beads inside the film. These results are quite consistent with the conclusion in our previous study that the adhesion behavior is strongly dependent on the mobility of the polymer film.

Acknowledgment. The authors thank T. Yamaue, M. Makino, and E. Nishitani for many helpful comments and discussions. This work is supported by The Japan Science and Technology Agency (JST).

REFERENCES

1. C. Creton, E. J. Kramer, H. R. Brown, and C.-Y. Hui, *Adv. Polym. Sci.*, **156**, 53 (2001).
2. L. Leger, E. Raphael, and H. Hervet, *Adv. Polym. Sci.*, **138**, 185 (1999).
3. M. Deruelle, L. Leger, and M. Tirrell, *Macromolecules*, **28**, 7419 (1995).
4. H. Morita, M. Yamada, T. Yamaguchi, and M. Doi, *Polym. J.*, **37**, 782, (2005).
5. S. T. Milner, T. A. Witten, and M. E. Cates, *Macromolecules*, **21**, 2610 (1988).
6. G. Grest, *Adv. Polym. Sci.*, **138**, 149 (1999).
7. M. Murat and G. S. Grest, *Phys. Rev. Lett.*, **63**, 1074 (1989).
8. M. Murat and G. S. Grest, *Macromolecules*, **22**, 4054 (1989).
9. G. S. Grest and M. Murat, *Macromolecules*, **26**, 3108 (1993).
10. A. R. C. Baljon, M. H. M. Van Weert, R. B. DeGraaff, and R. Khare, *Macromolecules*, **38**, 2391 (2005).
11. H. Morita, K. Tanaka, T. Kajiyama, T. Nishi, and M. Doi, *Macromolecules*, **39**, 6233 (2006).
12. K. Yoshimoto, S. J. Tushar, P. F. Nealey, and J. J. de Pablo, *J. Chem. Phys.*, **122**, 144712 (2005).
13. H. Morita, T. Ikehara, T. Nishi, and M. Doi, *Polym. J.*, **36**, 265 (2004).
14. S. W. Sides, G. S. Grest, M. J. Stevens, and S. J. Plimpton, *J. Polym. Sci., Part B: Polym. Phys.*, **42**, 199 (2004).
15. S. W. Sides, G. S. Grest, and M. J. Stevens, *Macromolecules*, **35**, 566 (2002).
16. S. W. Sides, G. S. Grest, and M. J. Stevens, *Phys. Rev. E: Stat., Nonlinear, Soft Matter Phys.*, **64**, 050802 (2001).
17. G. S. Grest and K. Kremer, *Phys. Rev. A: At., Mol., Opt. Phys.*, **33**, 3628 (1986).
18. K. Kremer and G. S. Grest, *J. Chem. Phys.*, **92**, 5057 (1990).
19. http://octa.jp
20. T. Aoyagi, F. Sawa T. Shoji, H. Fukunaga, J. Takimoto, and M. Doi, *Comput. Phys. Commun.*, **145**, 267 (2002).
21. M. L. Williams, R. F. Landel, and J. D. Ferry, *J. Am. Chem. Soc.*, **77**, 3701 (1955).